Kasetsart J. (Nat. Sci.) 48 : 637 - 650 (2014)

Heat Transfer Measurement on a Turbulent Spot Using the Energy Balance Method

Weerachai Chaiworapuek*, Suttaya Nongnoi and Chawalit Kittichaikarn

ABSTRACT

A turbulent spot is a small turbulent patch, surrounded by laminar flow at a boundary layer transition. It is an important mechanism, clearly showing the characteristics of highly turbulent flow and heat transfer inside the body. However, measurement in heat transfer from a flat plate to a fluid via a turbulent spot remains difficult due to the unsteady and unstable nature of the site. This paper detailed a temperature measurement technique using a coating of thermochromic liquid crystal. An analytical solution, derived from the developed energy balance method and an image processing technique were combined to visualize the thermal footprint of a turbulent spot. The experiment was performed over an isothermal flat plate in a low turbulence water tunnel where the turbulent intensity was lower than 1%. Reynolds number was initially kept at 75,000, as a reference rate for laminar flow. Transitional flow was bypassed by a small disturbance injection. The results were presented qualitatively and quantitatively using color, temperature, the heat transfer coefficient and heat flux as spots were propagated downstream. The locations of the leading and trailing edges were also clearly visualized. Turbulent spot information (spot celerities and the half spreading angle) were in agreement with those obtained by the other researchers, confirming the reliability of this technique. Thus, this energy balance method can be applied effectively to obtain insight into the bypass boundary layer transition over a flat plate.

Keywords: Heat balance method, turbulent spot, boundary layer transition, liquid crystals

NOMENCLATURE

B	Blue signal value
	Leading edge celerity of turbulent spots
C_{TE}	Trailing edge celerity of turbulent spots
C_{BC}	Celerity of becalmed region of turbulent spots
$\dot{E}_{in}$	Energy inflow (W)
$\dot{E}_g$	Energy source (W)
$\dot{E}_{st}$	Energy storage (W)
G	Green signal value
H	Hue signal value
h	Local convective heat transfer coefficient (W.K/m^2)
k	Thermal conductivity·(W.°C.m^{-1})
Nu_x	Local Nusselts number
Pr	Prandtl number
q	Heat flux (W.m^{-2})
q_l	Laminar heat flux, (W.m^{-2})
q_t	Turbulent heat flux, (W.m^{-2})
$\dot{q}$	Rate of heat transfer, (W)
R	Red signal value
Re_x	Local Reynolds number
δ_L	Laminar boundary layer thickness (mm)
ξ	Length of unheated starting section (m)

Department of Mechanical Engineering, Faculty of Engineering, Kasetsart University, Bangkok 10900, Thailand.
* Corresponding author, e-mail: chaiworw@hotmail.com

Received date : 20/03/14 Accepted date : 20/07/14

INTRODUCTION

The chaotic level of the flow over a flat plate basically depends on Reynolds number (Re), with the flow beginning as laminar and ending up as fully turbulent (Munson *et al.*, 2004). Transitional flow (between laminar and turbulent flow) was discovered first by Emmons (1951) who noticed a small turbulent patch on a water table that was later named a turbulent spot. It normally occurs when the flow is beyond a critical Reynolds number and as it propagates downstream, the turbulent spot expands relatively in both streamwise and spanwise directions so that a fully turbulent boundary layer will be fully formed after a combination of spots (White, 1986). Thus, the turbulent spot plays an important role in the flow and heat transfer characteristics during the laminar-turbulent transition process.

Following the initial description by Emmons (1951), experiments were undertaken by Schubauer and Klebanoff (1955). They found the existence of a "calmed region", following the trailing edge of the turbulent spot. This laminar area is located behind the spot and as turbulence decay occurs, the flow becomes steadily stable again. Later, many techniques were developed to visualize the shape of a turbulent spot (Elder, 1960; Cantwell *et al.*, 1978; Gad-El-Hak *et al.*, 1981; Perry *et al.*, 1981; Haidari and Smith, 1994); recently it has been claimed that it is triangular arrow head as shown in Figure 1 (Kittichaikarn, 1999). Moreover, there are some established parameters that can be used to explain the growth characteristics of a spot when it convects downstream. The propagation rates of the leading and trailing edges, later called turbulent spot celerity, were also obtained to show the velocities of different bounds (Schubauer and Klebanoff, 1955). Over many decades, variations in these parameters were found ranging from 0.74 to 0.88 at the leading edge and from 0.5 to 0.56 at the trailing edge; moreover, the turbulent spot half spreading angle (α), which has been used to explain the rate of growth of a turbulent spot, was reported to be in the range of 6-10° (Sankaran *et al*., 1988; Hofeldt, 1996; Kittichaikarn *et al*., 1999; Chong and Zhong, 2013).

"Liquid crystals" (LCs) are used to define a substance that has a combination of liquid and crystal properties. Historically, liquid crystals were first named by Lehmann (1889) who demonstrated that a liquid is birefringent, like crystals. Dabiri (2008) described the color changes in thermochromic LCs (one of the many different types of LCs) which can selectively reflect wavelength as a function of temperature, exhibiting a thick milky appearance at first and

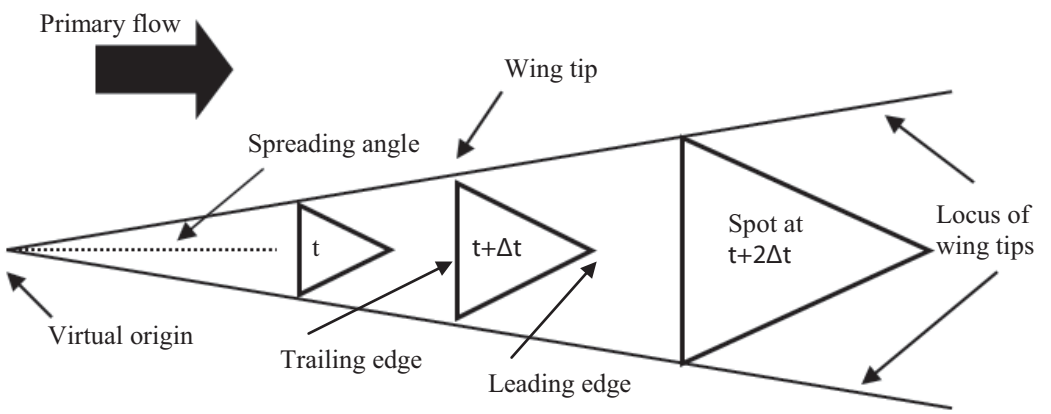

Figure 1 Growth characteristic of a turbulent spot, where *t* is the time after disturbing the flow by the spot generator (Kittichaikarn, 1999).

then, as the temperature reaches the lower limit of the color range, a black coated surface turns red. Reflecting light becomes yellow, green and blue when the surface is heated further. Above the upper limit, LCs become clear again. These color changes are reversible and repeatable if the temperature-sensitive liquid crystals are not physically damaged or chemically degraded. However, the hysteresis effect must be first checked as although its response time is only 3 ms, that is short enough for fluid problems to occur (Ireland and Jones, 1987). Before use as a temperature indicator, the color play-temperature relation should be defined via a calibration process, where the color change properties mainly depend on the prepared composition and manufacturing process. The selectable range starts from -30 and extends to 120°C in a bandwidth of 0.5°C to 20°C (Dabiri, 2008). Hence, thermochromic LCs have been used widely for temperature mapping in a variety of flow visualization applications (Stasiek and Kowalewski, 2002).

MATERIALS AND METHODS

This experiment was conducted in a water tunnel at the Computational Mechanics Laboratory, Kasetsart University. The test section was 0.2 × 0.15 m made from 10 mm thickness perspex to strengthen its structure. At an early stage, a particular flow was bled out to refresh the boundary layer along the leading edge of the flat plate as shown in Figure 2. A hot wire probe was installed at 800 mm from the leading edge for velocity and turbulence intensity measurement. At this point, the tunnel could produce a continuously laminar flow over the flat plate with Re varying from 45,000 to 200,000.

An aluminum plate 3 mm thick was chosen as a bottom wall due to its low weight and good thermal conductivity. The surface was heated using nine strip heaters below the test plate. All heaters were discretized and controlled using proportional-integral-derivative (PID) controllers. Local input signals for each PID were detected by three stations of type-K thin leaf thermocouples (model 88304;,Omega Engineering, Inc.; Stamford, CT, USA). These instruments were used to control the surface temperature. They were finely glued onto the top surface at 40, 60 and 78 mm from the leading edge to make up the isothermal test plate. Beneath each heater, a good thermal resistant plate

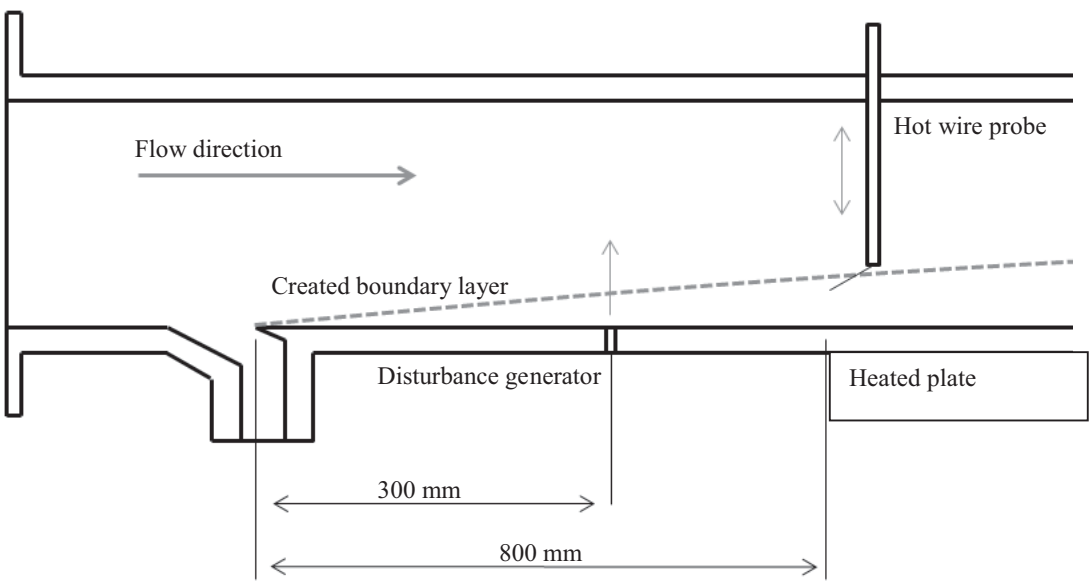

Figure 2 Water tunnel used for the study.

was laid to prevent unwanted power loss. A few thin, vertical aluminum plates were used to hold both the heaters and the insulation over the air gap as shown in Figure 3. In addition, a black plastic sheet 100 μm thick was firmly bonded onto the aluminum plate.

A spot generator was set up 300 mm downstream from the leading edge. This system was directly controlled by a programmable logic controller board. Instability was induced by injecting water through a 1 mm diameter hole using a solenoid valve. The induced flow was clearly characterized by liquid crystals, coated about 20 μm thick, on the top of the plastic sheet. The liquid crystals used in this research were of the Chiral Nematic type (Hallcrest; Glenview, IL, USA) and have an active color range of 2°C, from 27 to 29°C. On top of the crystals, a continuous, clear overcoat of varnish was applied to resist the degradation from the reflective properties of the water. Two 70 W fluorescent bulbs each with a diameter of 2.5 cm were assembled beside the test section as shown in Figure 3(b). Their white light, containing the required spectral wavelength from red to blue was directed to shine on the coated plate by glossy reflectors. For image acquisition, a video camera was installed 1.5 m above the test plate.

The experiment was carried out using a 2.5 HP high flow rate pump to supply a uniform freestream velocity of 0.17 $m.s^{-1}$, corresponding to an Re of 75,000 based on the plate length of 0.5 m. The measured turbulence intensity was lower than 1%. At the same point, the velocity profile under a laminar boundary layer, having a thickness (δ_L) of 8.2 mm was depicted as shown in Figure 4. It was similar to a Blasius profile.

ENERGY BALANCE METHOD

There are many analytical solutions of transient conduction that are suitable for three dimensional (3D) geometry. One of the most effective, developed from the finite difference

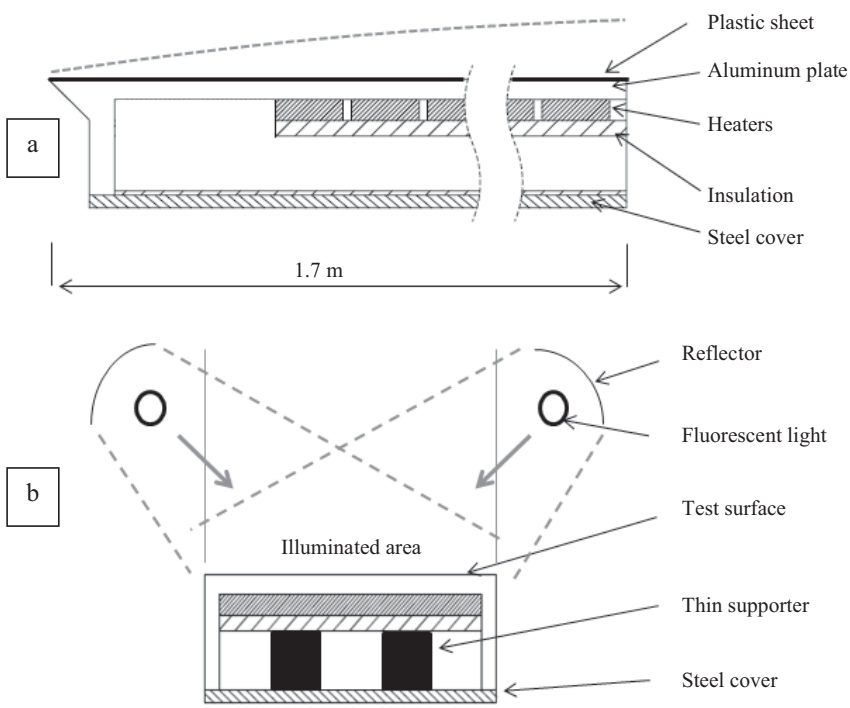

Figure 3 Preparation of heated plate: (a) Side view; and (b) Front view.

equations is called the energy balance method. This approach enables many different phenomena to be analyzed (Cengel, 2003; Incropera *et al*., 2007). It begins with Equation 1 regarding the conservation of energy:

$$\dot{E}_{in} + \dot{E}_g = \dot{E}_{st} \quad (1)$$

where terms are defined in the Nomenclature section at the beginning of the paper.

In this case, all heat flows are assumed to be "into the node" because the actual heat direction is unknown. In the 3D, flat plate analysis as shown in Figure 5, six adjacent nodes influenced the energy exchange on the central node without internal heat generation as shown in Equations 2–8:

$$\sum_{i=1}^{6} \dot{q}_{(i)\to(m,n,o)} = pC_p A \frac{\Delta z}{2} \cdot \frac{T_{m,n,o}^{t+\Delta t} - T_{m,n,o}^{t}}{\Delta t} \quad (2)$$

when :

$$\dot{q}_1 = \dot{q}_{(m-1,n,o)\to(m,n,o)} = k(\Delta y \cdot \frac{\Delta z}{2}) \cdot \frac{T_{m-1,n,o} - T_{m,n,o}}{\Delta x} \quad (3)$$

$$\dot{q}_2 = \dot{q}_{(m+1,n,o)\to(m,n,o)} = k(\Delta y \cdot \frac{\Delta z}{2}) \cdot \frac{T_{m+1,n,o} - T_{m,n,o}}{\Delta x} \quad (4)$$

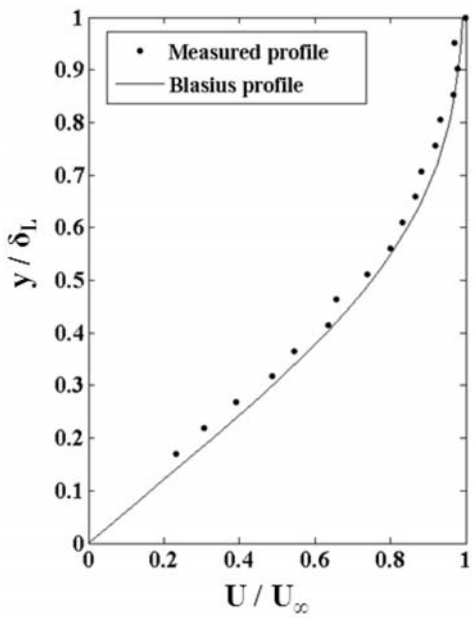

Figure 4 Measured boundary layer profile, where U is the measured velocity; U_α is the free stream velocity; y is the height of measuring position; δ_L is the thickness of the laminar boundary layer.

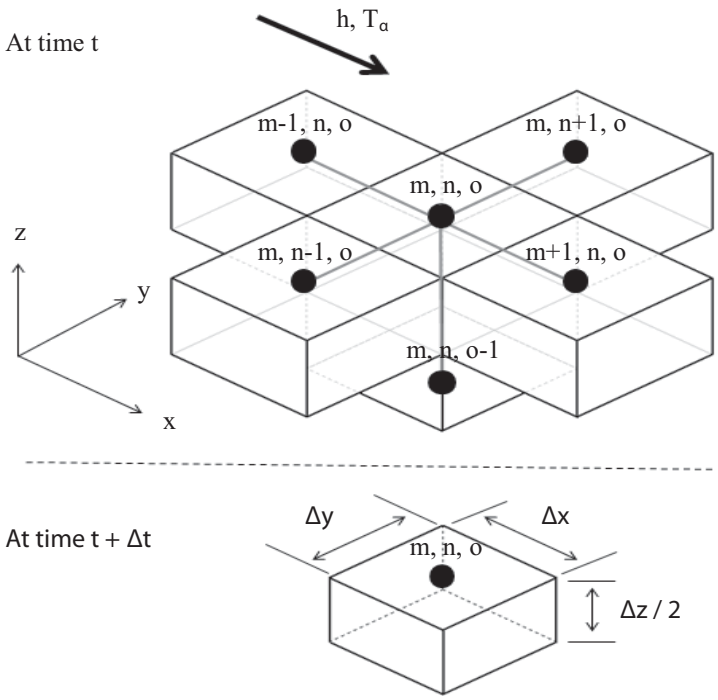

Figure 5 Map of adjoining nodes from the equation of conservation of energy (Equation 1) where h is the convective coefficient and T_α is the free stream temperature.

$$\dot{q}_3 = \dot{q}_{(m,n-1,o)\to(m,n,o)} = k(\Delta x \cdot \frac{\Delta z}{2}) \cdot \frac{T_{m,n-1,o} - T_{m,n,o}}{\Delta y} \quad (5)$$

$$\dot{q}_4 = \dot{q}_{(m,n+1,o)\to(m,n,o)} = k(\Delta x \cdot \frac{\Delta z}{2}) \cdot \frac{T_{m,n+1,o} - T_{m,n,o}}{\Delta y} \quad (6)$$

$$\dot{q}_5 = \dot{q}_{(m,n,o-1)\to(m,n,o)} = k(\Delta x \cdot \Delta y) \cdot \frac{T_{m,n,o-1} - T_{m,n,o}}{\Delta z} \quad (7)$$

$$\dot{q}_6 = h_x(\Delta x \cdot \Delta y) \cdot (T_\alpha - T_{m,n,o}) \quad (8)$$

where terms are defined in the Nomenclature section at the beginning of the paper.

The accurate temperature at each node can be directly obtained from the use of LCs. All elements that are illustrated in Figure 5 represent the black plastic sheet. The upper nodes are adjacent to the domain of the convective heat transfer by water. The lower nodes are laid on the heated aluminum sheet. However, this calculation is performed under the assumption that the temperature at the junction between the plastic sheet and the aluminum plate is constant. The temperature at this point can be approximated using the relation of heat conduction between two nodes as shown in Equations 9–11:

$$\dot{q} = k(\Delta x \cdot \Delta y) \cdot \frac{T_{m,n,o-1} - T_{m,n,o}}{\Delta z} \quad (9)$$

where $\dot{q}$ can be obtained from the formulation of unheated starting length as shown in Equation 10 :

$$Nu_x = \frac{0.332 \cdot \mathrm{Re}_x^{1/2} \cdot \mathrm{Pr}^{1/3}}{\left[1 - (\xi/x)\right]^{1/9}} \quad (10)$$

and in Equation 11:

$$q = h_x(T_{m,n,o} - T_\alpha) \quad (11)$$

where terms are defined in the Nomenclature section at the beginning of the paper.

In the present experiment, $T_{m,n,o\text{-}1}$ was obtained as 30°C. $T_{m,n,o}$ at a time of $t + \Delta t$ can be achieved from the same node of the next image. For example, if the 20th image is defined as an instantaneous event at a time of 2.8 s after injection from the spot generator, the 21st frame becomes the domain at a time of $t + \Delta t$. All rates of heat transfer from Equations 3–8 can be applied into Equation 2 to yield the heat transfer coefficients.

Image processing and color calibration

The images were grabbed at a frame rate of 25 images per second during the experiment. The recorded colors were defined as the percentages of red, green and blue, mixed together. Due to the numerical difficulty, the HSI (hue, saturation and intensity) color system was optionally proposed for improved understanding. However, only the H component refers to the color. Thus, the extracted data from experimental images could be converted to the H component as described by Paleebut and Kittichaikarn (2010) using Equations 12–14:

$$H = cos^{-1}(Z) \quad \text{if } G \geq R \quad (12)$$

$$H = 2¶ - cos^{-1}(Z) \quad \text{if } G < R \quad (13)$$

$$Z = \frac{\frac{2B - G - R}{2}}{\sqrt{(B-G)^2 + \frac{B-R}{G-R}}} \quad (14)$$

where terms are defined in the Nomenclature section at the beginning of the paper.

Before the test on the transitional flow was conducted, a calibration curve of the thermochromic liquid crystals (TLCs) must be performed. The visible spectra on the tested surface were collected by the recorders as the temperature was steadily elevated from 26.6 to 28.7°C in 0.3°C steps. An area of 7.8 × 7.8 mm, containing 20 × 20 pixels at the thermocouple tip was used to represent the surface temperature of the entire plate. It was found that hue images changed color from yellow to blue as the temperature increased. The hue signals and the temperatures were correlated as shown in Figure 6. This calibration curve was used to transform a color signal to a temperature.

From the calibration curve in Figure 6, the relationship between the fluid temperature and hue is given by Equation 15:

$$T = 58.48270856 \cdot H^3 - 61.24566302 \cdot H^2 + 23.15642190 \cdot H + 23.89758685 \quad (15)$$

where T is the temperature in degrees Celcius and H is the hue value.

The goodness of fit (R^2) for Equation 15 was 0.99873. The surface temperature was kept

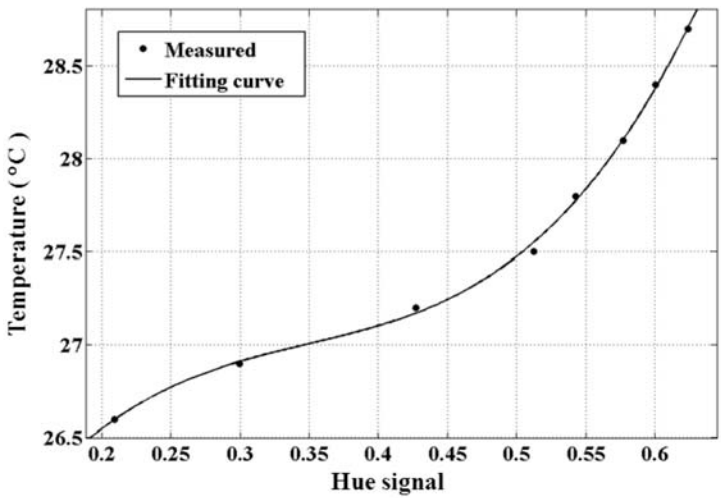

Figure 6 Relationship between hue and temperature on calibration curve.

constant at 28.7°C which was the upper limit of the color range. Beyond this point, TLCs show hysteresis.

RESULTS AND DISCUSSION

Thermal characteristics of turbulent spot

The series of RGB images of the turbulent spot, convecting downstream from left to right are depicted in Figure 7 over a time period of 6 s. The chosen time interval was set at 0.8 s, starting from 2.8 s up to 6.0 s after injecting the disturbance. All consecutive images were grabbed from 0.5 to 0.84 m in a streamwise direction. In the spanwise direction, zero distance was set at the center and spanned out about 0.05 m on each side. From the images, the hue signals gave a clear vision of the streaky structure of the turbulent spot as shown in Figure 8.

Before the spot arrival, the test surface was maintained uniformly blue at the highest temperature of 28.5°C. It later turned to green streaks which represented the lower temperature underneath the incoming turbulent spot. A long trail behind the green streaks, named the "becalmed region" can also seen. It is a closed area where the turbulent boundary layer returns to the initially stable laminar condition (Schubauer and Klebanoff, 1955). Figure 9 depicts the temperature distribution on the heated plate in the streamwise and spanwise directions that was accurately converted from the calibrated relation. It was found that, in this condition, a spot could generally reduce the temperature of the heated plate by approximately 0.4°C. The lowest temperature was noted at the center of each streak. For example, in Figure 9 at t = 6 s, the lowest temperature could be measured at 27.4°C and the further the spot moved, the larger the area of the cooler temperature. Thus, all temperature distributions found at most downstream locations in Figure 9 appear similar to those appearing in the turbulent boundary layer. This was clear evidence that confirmed the higher rate of heat transfer within a spot's streaky structure.

An analytical formula, derived from the energy balance method as explained previously, was then used to yield the convective heat transfer coefficient and instantaneous heat flux beneath the spots. The series of calculated convective heat transfer coefficients are illustrated in Figure 10. It was found that the arrival of a turbulent spot improved the ability to identify heat transfer from the color bar. The contours showed that the

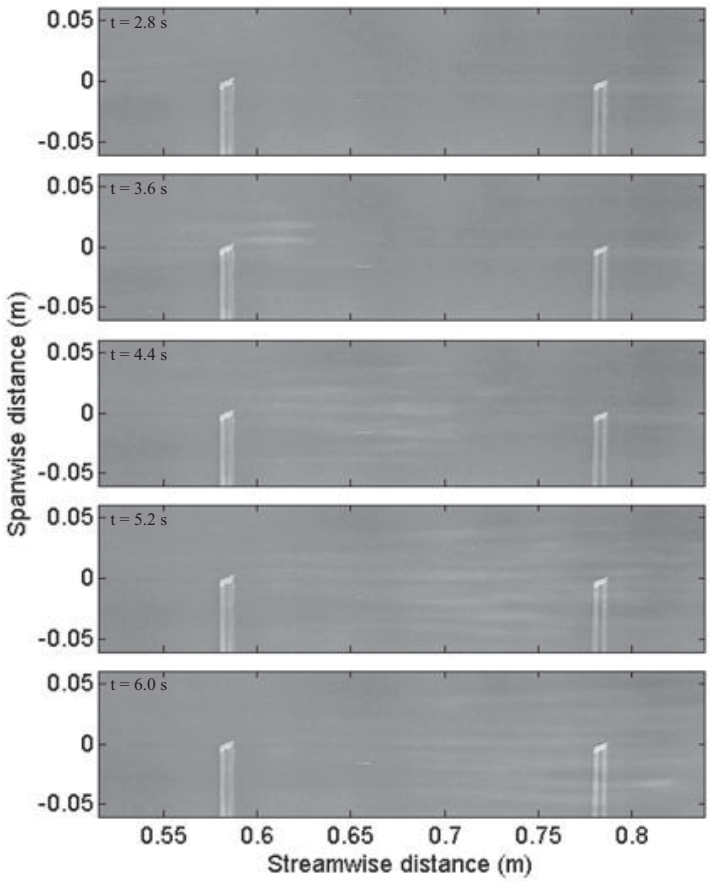

Figure 7 Red-green-blue signal as spot moves downstream with interval time of 0.8 s.

convective heat transfer coefficient in the core of each streak appeared between 400 and 500 W.K.m^{-2} and reached 600–700 W.K/m^{-2} when it reached the fully turbulent region. The position of the maximum convective coefficient was generally located inside all streaks. This gave good agreement with the contours of temperature distribution as the greater the heat transfer coefficient, the greater was the cooled temperature.

Evolution of spot footprint

When all the convective coefficients were inserted into Equation 8, the spatial heat flux distribution that transferred from the heated surface to the fluid at freestream was obtained. Figure 11 shows the heat flux distribution beneath the turbulent spot, convecting downstream with a time interval of 0.8 s. The relative values presented only as the heat flux of the turbulent part are provided in Equation 12:

$$q_t = q = q_l \quad (12)$$

where terms are defined in the Nomenclature section at the beginning of the paper.

The boundary was plotted with the value of the heat flux set to 10%. As the spot traveled from left to right, quantitative and qualitative information in the streamwise and spanwise directions were provided. During the experiment, it was found that the incoming streaks of a turbulent spot were randomly located due to the spot being unsteady and unstable. All observed streaky structures were induced by the effect of hairpin vortices not only in the streamwise direction but also in the spanwise direction. For example, the leading edge of the turbulent spot first appeared as small unstable areas at the most

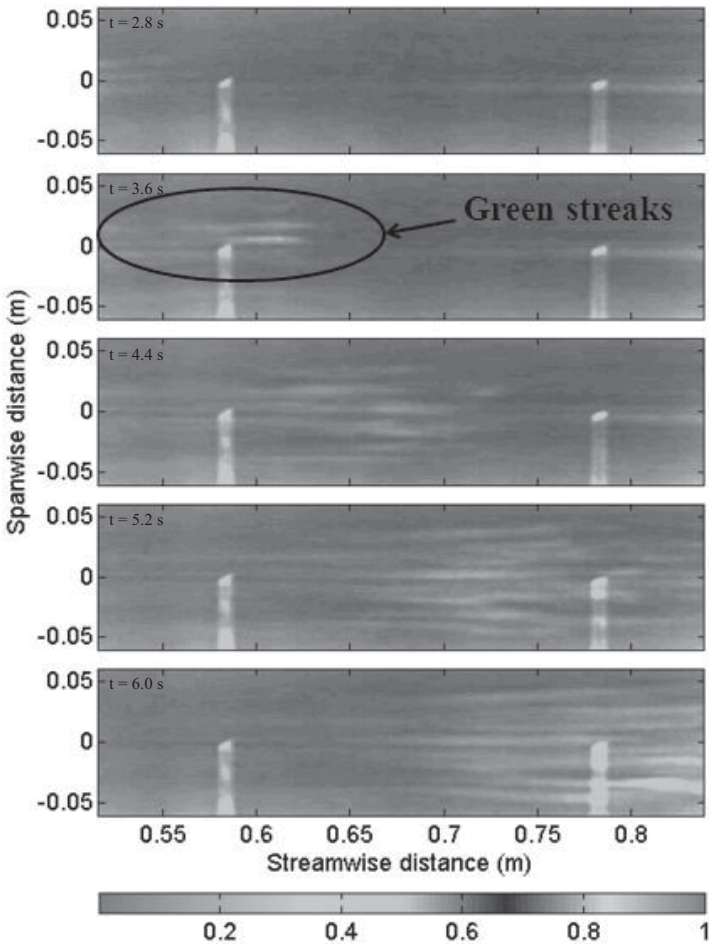

Figure 8 Hue signal (0.2–1) as spot moves downstream with time interval of 0.8 s.

downstream location, later becoming the main streaky structure of the body. This occurred by the arrival of the primary hairpin-like vortex that brought colder water near the upper edge of the boundary layer down to the heated surface (Haidari and Smith, 1994). In addition, in the spanwise direction, the formation of a small turbulence structure, shown at point A in Figure 11 at time t = 3.6 s, was caused by vortices. Later, it became a main part of spot's side wing in the next frame (time t = 4.4 s), resulting in the spanwise growth of the structure. The position of a trailing edge depended on the location of the highest heat flux inside spot, represented by a black wavy line in Figure 11. The virtual trailing edge was located by fitting all positions in the streamwise direction of the wavy line inside spots. Wing tips were defined where the wavy line reached each side of the spot laterally as, for example at points B and C in Figure 11. These wing tips were used to determine the half spreading angle and propagation rate of the trailing edge of the spot. Behind the trailing edge, a becalmed region existed at the rear of the spot. However, it was found that the turbulent spot trailing in the spatial and temporal heat flux distribution was shorter than in the temperature distribution. The longer trail was caused by the effect of remained storage energy in the plastic sheet that was expressed as a delayed temperature change, even after the spot had already passed. This distorted the shape of the becalmed region on the temperature distribution. However, this

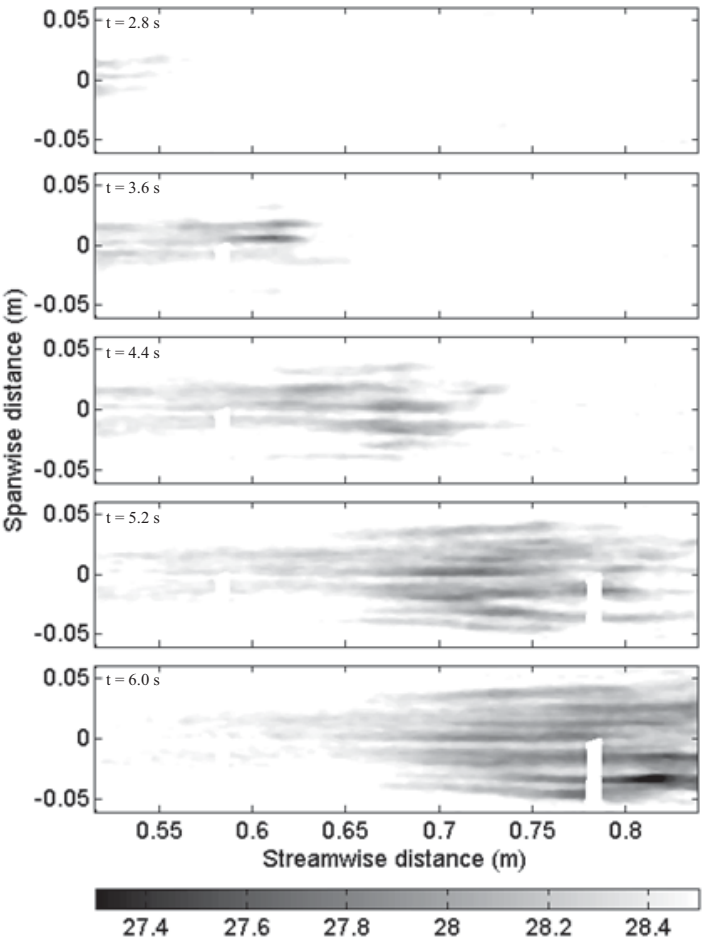

Figure 9 Spatial temperature distribution (27.4–28.4°C) as spot moves downstream with time interval of 0.8 s.

effect could be eliminated after the heat balance method was applied. Hence, the true shape of the turbulent spot could be revealed on the heat flux images. This clearly supported the hypothesis by Kittichaikarn *et al*. (1999) of the wrong shape in the becalmed region being detected by temperature measurement.

The measured heat flux, generated by the turbulent spot in the current study was generally 200–400 $W.m^{-2}$. At the core of each streak, it was approximately 600–750 $W.m^{-2}$ and up to 1,200 $W.m^{-2}$ when the spot became fully turbulent. From the combined results above, it can be concluded that the existence of a turbulent spot has two main parts consisting of the body of the turbulent spot, surrounded by the boundary of a leading edge and trailing edge. This part has an "arrow head" shape as seen in Figure 12. The second part is the becalmed region occurring behind the body of the spot.

Turbulent spot parameters

Table 1 summarizes the turbulent spot parameters including the turbulent spot celerities at the leading edge, trailing edge and half spreading angle (α) from the present study, compared to some published data. All shown data were measured at a height of $0 \leq y/\delta_L \leq 0.35$, where y is the height of

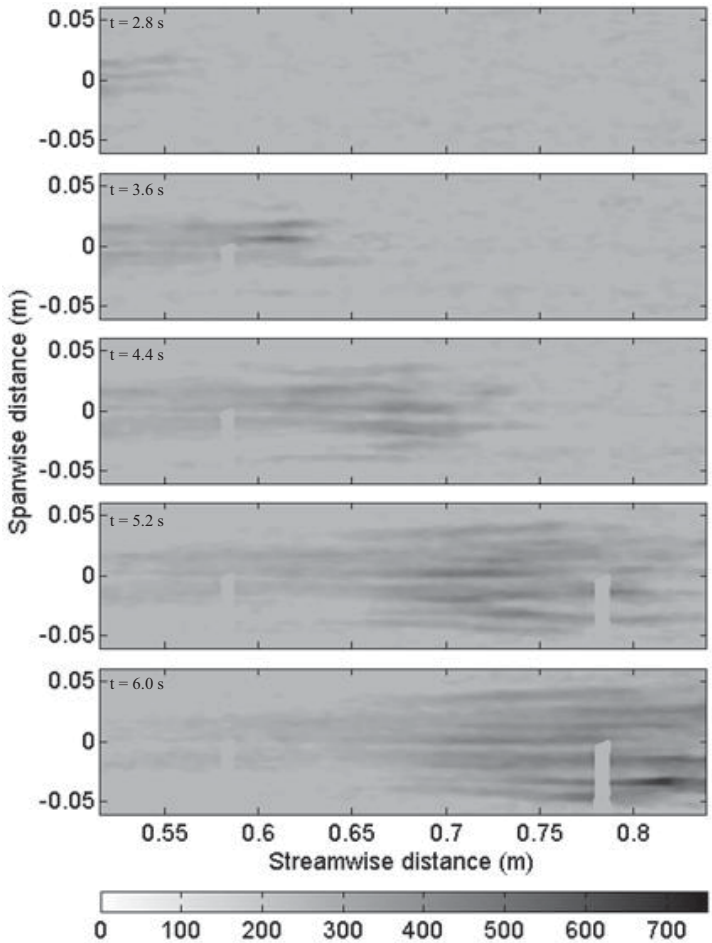

Figure 10 Spatial heat transfer coefficient distribution (0–700) as spot moves downstream with time interval of 0.8 s.

Table 1 Turbulent spot parameters of leading edge celerity (C_{LE}), trailing edge celerity (C_{TE}) and half spreading angle (α) obtained from the current study and other published research.

Data source	C_{LE}	C_{TE}	$\alpha°$
Schubauer and Klebanoff (1955)	0.88	0.50	10.0
Sankaran *et al*. (1988)	0.74	0.53	9.0
Hofeldt (1996)	0.88	0.56	10.0
Chong and Zhong (2005)	0.83	0.54	8.6
Kittichaikarn *et al*. (1999)	0.83	0.56	6.0
Current study	0.78	0.53	5.5

the measuring position. The location of the leading edge, trailing edge and half spreading angle were identified as explained above. In the current study, this calculation assumed that all parameters were linear as spots propagated downstream.

In the current study, the turbulent spots propagated downstream at a velocity of 78% and 53% of freestream velocity at leading and trailing edges, respectively. These results were consistent with those produced by other researchers. It should

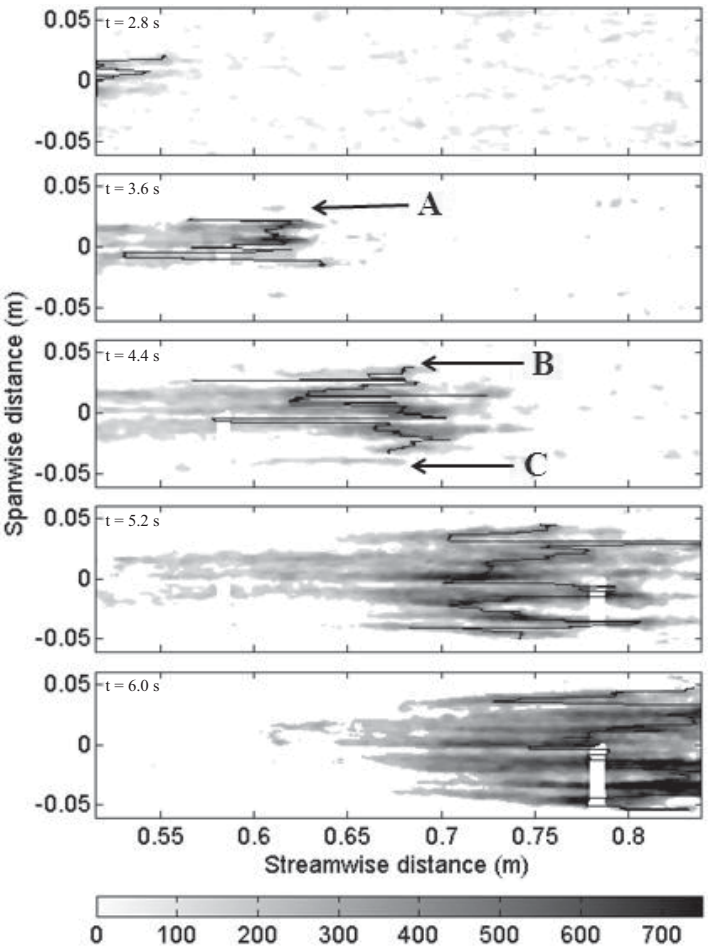

Figure 11 Spatial heat flux distribution as spot moves downstream with time interval of 0.8 s. A, B and C represent a small turbulence structure and its two wing tips, respectively.

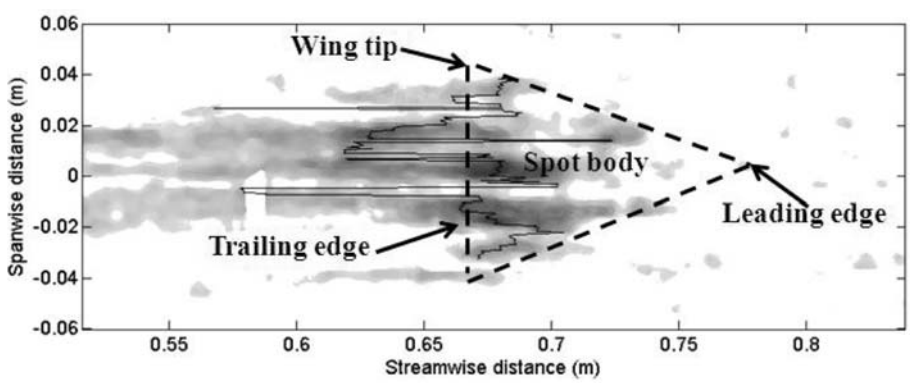

Figure 12 Deduced "arrow head" shape of a turbulent spot.

be noted that turbulent spots moved faster on the leading edge than on the trailing edge. Thus, this difference caused spot growth in a streamwise direction. Compared to data from the other studies in Table 1, the obtained α in the current study was less. However, the difference from the result of Hofeldt (1996) may have resulted from the presence of a young turbulent spot, which was responsible for the smaller half spreading angle. This was initially investigated by Kittichaikarn *et al*. (1999). Furthermore, it should be noted that all data except from Kittichaikarn *et al*. (1999) and the current study were measured at a location of y/δ_L below 0.35 but not exactly on the surface. This observation was confirmed by Chong and Zhong (2013) that a large gradient of the half spreading angle of a spot occurred at the near wall region under the boundary layer. By comparison with classical turbulent spots, especially those presented by Kittichaikarn *et al*. (1999), it was also found that all turbulent spot characteristics and parameters, obtained via the heat balance method were validated. Therefore, the analytical method used in the current study is capable of being used for heat transfer measurement on turbulent spots.

CONCLUSION

The present analytical technique provided an accurate predictive solution of the convective heat transfer coefficient and heat flux over an unsteady heated surface. This method was derived from the finite difference equations using an energy balance approach. This experiment was used to detect the development of an artificially created turbulent spot under a bypassed boundary layer transition under a zero pressure gradient.

It was found that the formation and characteristics of turbulent spots, governed by this energy balance method, had good agreement with most comparable data from other researchers. Furthermore, all the spot parameters determined in the current study (the propagation rate at the leading and trailing edges and the half spreading angle) were similar to those obtained from other published data. Based on the performance and accuracy, the analytical solution presented in this study can be counted as an effective predictive technique for both heat flux and the convective coefficient. Therefore, it can be applied to not only the subject of turbulent spots but also many other thermal applications that involve unsteady phenomena.

However, further investigation is recommended on the becalmed region and on young turbulent spots as this will strengthen the evidence to develop an improved transition model that can be used to predict heat transfer along a boundary layer transition.

ACKNOWLEDGEMENT

The authors gratefully acknowledge the financial support by the Kasetsart University Research and Development Institute (KURDI).

LITERATURE CITED

Cantwell, B., D. Coles and P. Dimotakis. 1978. Structure and entrainment in the plane of symmetry of a turbulent spot. **J. Fluid Mech.** 87(4): 641–672.

Cengel, Y.A. 2003. **Heat Transfer: A Practical Approach.** 2nd ed. McGraw-Hill. New York, NY, USA. 932 pp.

Chong, T.P. and S. Zhong. 2005. On the three-dimensional structure of turbulent spots. **J. Turbomach.** 127: 545–551.

Chong, T.P. and S. Zhong. 2013. On the shear stress and thermal footprints of turbulent spots at zero pressure gradient. **J. Mech. Sci. & Tech.** 27(4): 1001–1009.

Dabiri D. 2008. Digital particle image thermometry/velocimetry: a review. **Exp. Fluids.** 46(2): 191–241.

Elder, J.W. 1960. An experimental investigation of turbulent spots and breakdown to turbulence. **J. Fluid Mech.** 9(2): 235–246.

Emmons, H.W. 1951. The laminar-turbulent transition in a boundary layer-part I. **J. Aerosp. Sci.** 18: 490–498.

Gad-El-Hak M., R.F. Blackwelder and J.J. Riley. 1981. On the growth of turbulent regions in laminar boundary layers. **J. Fluid Mech.** 110: 73–95.

Hofeldt, A. 1996. **An Investigation of Naturally-Occurring Turbulent Spots using Thin-Film Gauges.** Doctoral thesis, University of Oxford. Oxford, UK.

Haidari, A.H. and C.R. Smith. 1994. The generation and regeneration of single hairpin vortices. **J. Fluid Mech.** 277: 135–162.

Incropera, F.P., D.P. Dewitt, T.L. Bergman and A.S. Lavine. 2007. **Fundamentals of Heat and Mass Transfer.** 6th ed. John Wiley & Sons. Hoboken, NJ, USA. 925 pp.

Ireland, P.T. and T.V. Jones. 1987. The response time of a surface thermometer employing encapsulated thermochromic liquid crystals. **J. Phys. E: Sci. Instru.** 20: 1195–1199.

Kittichaikarn, C. 1999. **A Study of Turbulent Spots and Wake Induced Transition Using Liquid Crystals.** Doctoral thesis, University of Oxford. Oxford, UK.

Kittichaikarn, C., P.T. Ireland, S. Zhong and H.P. Hodson. 1999. An investigation on the onset of wake-induced transition and turbulent spot production rate using thermochromic liquid crystal. *In* **Proceedings of 44th ASME International Gas Turbine and Aeroengine Congress and Exposition,** 7–10 June 1999. Indianapolis, IN, USA.

Lehmann, O. 1889. Über fliessende krystalle. **Z. Phys. Chem.** 4: 462–472. [in German].

Munson, B.R., D.F. Young and T.H. Okiishi. 2004. **Fundamentals of Fluid Mechanics.** 5th ed. John Wiley & Sons. Hoboken, NJ, USA. 772 pp.

Paleebut, A.M. and C. Kittichaikarn. 2010. The effect of a swirl on the heat transfer coefficient of flow in a rectangular duct using thermochromic liquid crystals. **J. Flow Vis. & Image Proc.** 17(3): 255–266.

Perry A.E., T.T. Lim and E.W. Teh. 1981. A visual study of turbulent spots. **J. Fluid Mech.** 104: 387–405.

Sankaran, R., M. Sokolov and R.A. Anthonia. 1988. Substructures in a turbulent spot. **J. Fluid Mech.** 197: 389–414.

Schubauer, G.B. and P.S. Klebanoff. 1955. **Contributions on the Mechanics of Boundary Layer Transition.** National Advisory Committee for Aeronautics Technical Note 3489. Washington, DC, USA. 31 pp.

Stasiek J.A. and T.A. Kowalewski. 2002. Thermochromic liquid crystals applied for heat transfer research. **Opto-Electron. Rev.** 10(1): 1–10.

White, F.M. 1986. **Fluid Mechanics.** 2nd ed. McGraw-Hill. New York, NY, USA. 732 pp.